Measurements and modeling of electron energy distributions in the afterglow of a pulsed discharge in BF_3

To cite this article: Ž. Nikitović *et al* 2011 *EPL* **95** 45003

A Letters Journal Exploring the Frontiers of Physics

August 2011

EPL, **95** (2011) 45003
doi: 10.1209/0295-5075/95/45003

www.epljournal.org

Measurements and modeling of electron energy distributions in the afterglow of a pulsed discharge in BF_3

Ž. Nikitović[1], S. Radovanov[2], L. Godet[2], Z. Raspopović[1], O. Šašić[1,3], V. Stojanović[1] and Z. Lj. Petrović[1(a)]

[1] *Institute of Physics, University of Belgrade - POB 68, 11080 Belgrade, Serbia*
[2] *Varian Semiconductor Equipment Associates - 35 Dory Road, GL-17, Gloucester, MA 01930, USA*
[3] *Faculty of Transport and Traffic Engineering, University of Belgrade - Belgrade, Serbia*

received 29 March 2011; accepted 8 July 2011
published online 5 August 2011

PACS 52.20.-j – Elementary processes in plasmas
PACS 52.20.Fs – Electron collisions
PACS 52.65.Pp – Monte Carlo methods

Abstract – In this paper we use experimental data (Radovanov S. and Godet L., *J. Phys.: Conf. Ser.*, **71** (2007) 012014) for time-resolved electron energy distribution function in boron trifluoride (BF_3) discharges together with cross-sections for electron excitation processes and attachment in order to explain electron dynamics in the pulsed plasma doping system. A Monte Carlo simulation (MCS) was used to perform calculations of the electron energy probability function (EEPF) in pulsed DC electric fields as found in practical implantation devices. It was found that in the afterglow, electric field in the plasma is not zero but still has a significant reduced electric field (E/N) albeit below the breakdown condition. Our analysis assuming free diffusion conditions in the afterglow led to the calculation of EEPF for a range of E/N corresponding to different afterglow times of a pulsed DC discharge. Calculated and experimental EEPF agree fairly well for a given set of cross-sections (see paper by Radovanov and Godet quoted above) and assumed initial distributions. In addition we have modeled the kinetics of production of negative ions in the afterglow as observed by experiment and found an increase in the production of negative ions in the early afterglow. Electron attachment in BF_3 with 0.1% of F_2 is a possible explanation for the observed rate of negative-ion production as predicted by our Monte Carlo simulation. However, the most likely cause for the increase in detected number density of ions is the collapse of the field-controlling electrons.

Introduction. – In order to achieve precise boron dopant placement in the silicon, a DC pulsed plasma doping system (PLAD) through BF_3 is commonly used. Requirement is that it must produce a uniform plasma and subsequent implantation with normal ion incidence. Additionally, the shape of the ion density profile can be affected by using different anode-to-cathode distances and a hollow cathode that provides additional high-energy electrons to the bulk plasma.

Such system is capable of high dose rates at energies ranging from ultra low to moderate (0.02–10 kV). Pulsed plasma is generated adjacent to the silicon wafer using pulsed power supply. Typical pulse widths range between 5 and 50 μs, and pulse repetition rates between 100 and 10000 Hz.

Time-resolved probe measurement showed that cold plasma is being produced both during the discharge and during the afterglow, which may play an important role in the process control to facilitate extraction of ions.

It was previously found that BF_2^+ is the dominant ion species, with BF^+ as the second most abundant ion species [1]. Using negative ions increases the efficiency of ion sources and hence one of the reasons to employ pulsed plasmas and extraction during the afterglow. As shown in this paper our experiments also indicate the importance of low-energy electron attachment in the BF_3 mixture as found in PLAD sources with all the possible products of dissociation.

It is well understood that the electron energy distribution function provides information on the kinetics of plasma production and the concentration of ions and reactive species that result from the balance between

(a) E-mail: zoran@ipb.ac.rs

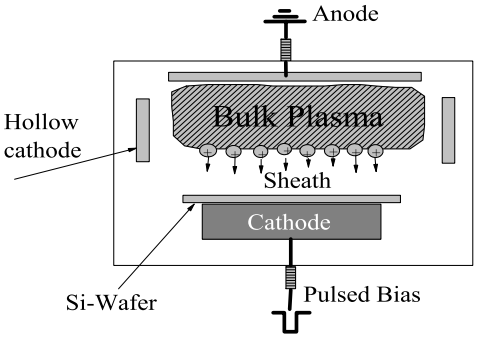

Fig. 1: Principle of PLAD.

production and loss processes in the discharge. In this paper we discuss the time evolution of the electron energy probability function (EEPF) in a pulsed plasma doping system and how it affects kinetics of some processes. We have performed measurements of EEPF during the ON and OFF period of the discharge. The goal is to follow the kinetics of electrons in a free diffusion regime in the afterglow and to test to which degree one may predict some of the resulting atomic and molecular collision processes. Most importantly we try to explain relatively high electron energies found in the afterglow.

Experimental. – Probe measurements in the bulk region of the discharge reported here are conceptually the same as in our previous work [2]. The main chamber was made of aluminum and could be pumped down to a base pressure around 2×10^{-7} torr. A vacuum load-lock was attached to the main chamber for the 300 mm wafer handling. Process gases such as BF_3, Ar or their mixtures are introduced through a shower head gas inlet system. The experimental set-up is shown in fig. 1.

During the plasma doping process, the chamber could be maintained at a pressure between 10 and 300 mtorr by a closed-loop pressure control system. The 300 mm silicon wafer was placed on a wafer chuck and was electrically isolated from the chamber.

The pulsed plasma was produced between two parallel electrodes: the cathode (including the silicon wafer) and the anode. During the plasma implantation, the output of a high-voltage pulsed DC power supply was connected to the wafer chuck. The negative voltage formed a sheath between the cathode and the bulk plasma and accelerated positive ion species in the plasma toward the wafer. The negative-bias voltage used in this study was provided by a 0–5 kV power supply with pulse-ON time of 20–40 μs and pulse-OFF time of 0.5–2.0 ms, *i.e.*, a 1–8% duty ratio. The gap between electrodes was adjusted according to the required E/N and operating conditions between 3 cm and 12 cm. During the pulse peak current was 0.25 A–0.5 A and the corresponding electron density was $1 \cdot 10^9$–$5 \cdot 10^9$ cm^{-3}. During the OFF period (afterglow) the density was typically ten times lower and decayed rapidly. For bulk plasma diagnostics and time-resolved measurements, the wafer chuck was negatively biased, while the anode plate as well as the ion mass and energy analyzer were held at ground potential. Experimental results for the EEPF are given for the relatively short voltage pulse on time 30 μs and low duty ratio (1.0%) at the pulsed frequency of 2.5 kHz.

The single-sided cylindrical Langmuir probe was used to measure the pulsed plasma characteristics. The probe was inserted from the side of the chamber, and it traveled in a radial direction from the edge to the center of the wafer. The probe diameter was 100 μm and its length 1 cm and the probe head was facing 90° from its axis and could be rotated in every 45° so that it could face toward the wafer, anode or the chamber walls as needed. The vertical distance between the probe surface and the wafer surface was approximately 3.7 cm when the probe was facing the side wall, 3.1 cm when facing the wafer, and 4.3 cm when facing the anode. A commercially available bipolar power supply, BOP 1000M from Kepco, was used for the automatic voltage sweep. For the probe diagnostics, the probe bias was scanned typically between −500 V and 50 V with the voltage step of 0.1 V. A linear amplifier built on Agilent's analog Optocoupler (HCNR201) was used to measure the probe current at different biases. Description of this amplifier can be found elsewhere [3]. The output signal from the amplifier was connected to a Boxcar Averager unit for gated integration. For time-resolved plasma diagnostics from the initial plasma ignition to the end of the afterglow period, the sampling width of the Boxcar Averager was fixed at 0.1 μs, and the delay was varied between 1 μs and 2 ms. Due to the pulse rise time and intrinsic time delays in electronics, we expected a few μs of uncertainty in the timing.

The analysis of the I-V characteristics was based on the assumptions that the mean-free path of the electrons is much larger than the Debye shielding length, and that the electrons have a Maxwellian distribution and background ions are cold [4]. The first assumption is valid under our experimental conditions [2], while the second argument while often used in the literature is not easily validated. In fact a non-Maxwellian distribution was obtained during the pulse-ON period. The effect of fast electrons in measuring n_e and T_e was introduced. The fast electron analysis is based here on the Laframbois theory which calculates the values of kT_e and density of fast electrons in the region where the bias voltage on the probe is close to the plasma potential so that energetic electrons can cross the potential barrier [5]. This analysis assumes the knowledge of the bulk electron contribution and ion contribution to the probe current measurement. In these experiments the time evolution of the other plasma parameters such as plasma potential, ion density and electron temperature, was obtained. The plasma potentials in the afterglow were extracted also from the I (Vb) measurement. The time-averaging procedure for the accumulated time-resolved signal detection was done using the gated integration as described above.

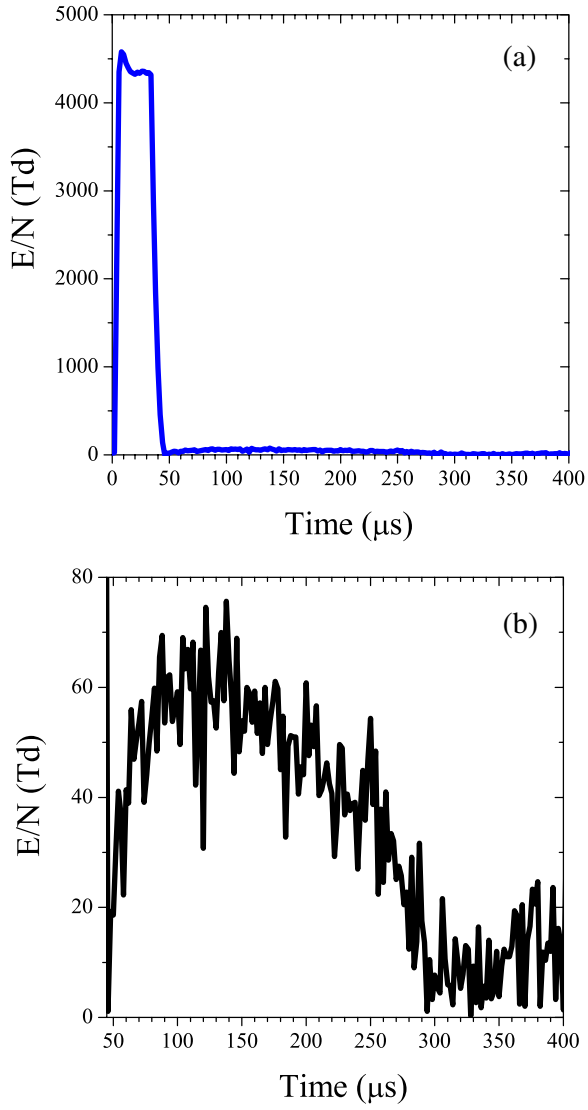

Fig. 2: (Colour on-line) (a) Full relaxation of EEPF in BF_3 (EXP). (b) Relaxation in the background E field (EXP). A cathode bias of -1 kV, a 30 μs pulse duration and 2500 Hz pulse frequency are applied between the anode and the cathode. The pressure was 60 mtorr and the BF_3 gas was fed through mass flow controller at gas flow of 5 sccm.

Experimental results and discussion. – At the beginning of each cycle the high-voltage pulse has a short period of overshoot due to the need to achieve breakdown and create the plasma. Later on, the voltage reaches the stable operating value. Here we show in fig. 2(a) the voltage pulse during the ON period and the OFF period as well. The discharge lasts around 30 μs. We have represented the voltage pulse through effective E/N that would exist without the space charge shielding. It is obvious that in the actual plasma the field is high only in the sheaths. After the field is turned off the voltage (E/N) reduces close to the zero value only to pick up and be significant before 100 μs as seen in fig. 2(b) peaking at 150 μs at around 80 Td. The afterglow electric field may also be described as an overshoot voltage partially caused by the operation of a non-ideal power supply [4]. This relatively high residual voltage causes a relatively high E/N during the afterglow that may affect the electron energy distribution.

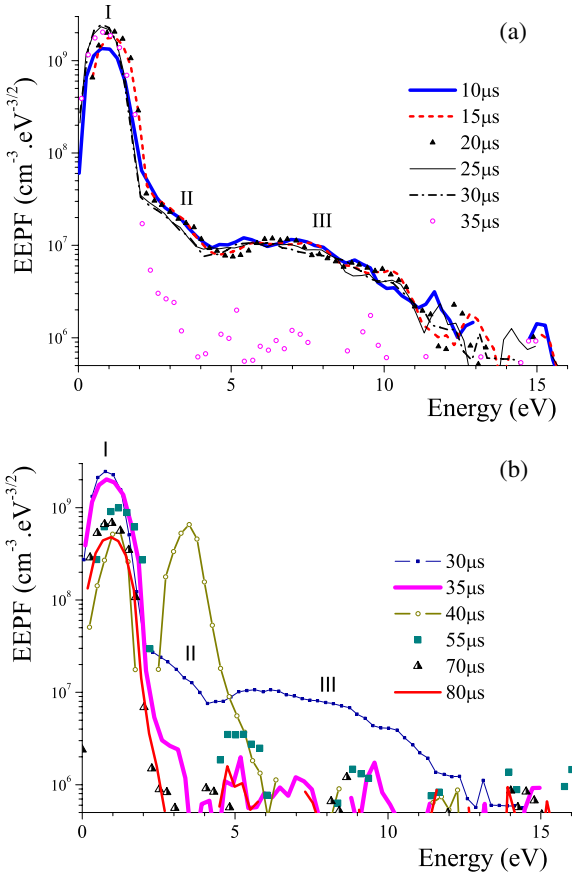

Fig. 3: (Colour on-line) Time evolution of the electron energy probability function. During the pulse-ON period (a) and during the afterglow (b) (EXP).

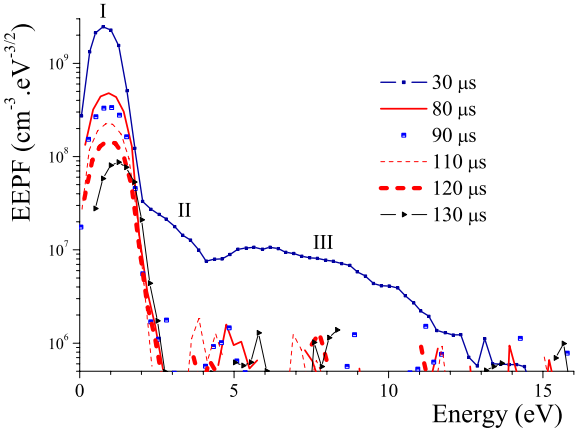

Fig. 4: (Colour on-line) Time evolution of the electron energy probability function in the afterglow. The measurements were made for 60 mtorr.

Measured electron energy probability functions (EEPF) [6] are in figs. 3 and 4 and represent the electron

during the ON period and relaxation during the OFF period obtained at a gas pressure of 60 mtorr. Measurements were made, as explained earlier by the Langmuir probe.

Kinetics of electrons during the discharge and afterglow —comparisons of model and experiment. – A very high electric field across the cathode sheath during the high-voltage pulse breakdown (ON period) provides energy for electrons to ionize and sustain plasma but it may also induce a non-local character of the EEPF in the sheath. EEPF during high-voltage pulse at a fixed position of the probe in the bulk of the discharge is shown in fig. 3 for 10–30 μs. A slight increase of the low-energy part of the EEPF for 25 μs and 30 μs (region I in fig. 3) is the result of the increased ionization efficiency in the second part of the pulse, *i.e.* where sheath expansion toward the Child-Langmuir limit proceeds in a time of the order of 10 μs. Mean energy decreases during the same time period. One may expect that by rising the voltage and expanding the sheath, very-high-energy electrons escape towards walls and only low-energy electrons are collected by the probe. It is important to conclude here that the shape of the EEPF is consistent with a mean energy of 2.9 eV with several peaks and throughs at higher energies showing an inherently non-equilibrium nature of the discharge and the effect of inelastic processes and acceleration of electrons in sheaths.

The measured EEPFs showed that the population of low-energy electrons decreases at the beginning of the OFF period while a moderately high electron-energy population between 1 and 2.5 eV remains almost the same. This results in an increase of the electron mean energy. The decrease of the low-energy part of the EEPF after the pulse is turned off is a result of insignificant electron multiplication due to the sudden loss of very-high-energy electrons (> 3 eV) to the walls during the sheath collapse. At the energies below 1.5 eV EEPF does not show characteristics of a Maxwellian although the slope up to about 2 eV (region I in figs. 3 and 4) may be fitted by a Maxwellian.

The persistence of the higher-mean-energy EEPF (as measured in the experiment) at around 1–2 eV and at times beyond 100 μs is surprising and has been only explained by the residual high E/N in the afterglow period. To test this and explain the experimental data we have made model calculations.

The hydrodynamic description of electron swarm for the conditions shown in fig. 4 reveals [7] that the combination of first, third and harmonic vibrational excitation resonances results in a broad plateau above 4 eV and below the threshold for electron impact ionization (region 3) in figs. 3 and 4 reflects various electron energy loss processes. Some of them result in peaks being observed in the EEPF recorded in the afterglow.

Model calculations for electron EEPF in the afterglow. – Electron attachment that have high threshold (10 eV) with respect to the mean electron energy is not affecting steady-state parameters due to the significant ionization in these conditions. On the other hand, complete depletion in EEPF for all afterglow curves indicates insignificant electron production by ionization while electron attachment comes out as an important electron energy loss channel. At low gas pressures one may expect that diffusion to walls is the main loss mechanism. In the afterglow, the residual field (fig. 2(b)) high-energy electrons are soon absorbed to the walls leaving slow electrons between the electrodes. In weakly electronegative BF_3 discharge negative ions are trapped within the space charge field thus reducing the plasma potential and further increasing electron diffusion to the walls. This situation is exemplified by lines denoting times of 30 and 35 μs in fig. 3 and greater where significant and selective high-energy electron depletion is notified.

In BF_3 plasma, the BF_2^+ diffusion, electron ion recombination, charge exchange and electron attachment may also contribute to the decay process.

The basis of model is that the kinetics of electrons is assumed to be that of a swarm or in other words of a free diffusion. One could perhaps estimate the time for achieving the free diffusion (merely by diffusion losses) and we based our estimate by scaling the times calculated for nitrogen and argon [8]. For 60 mtorr the discharge estimated time to achieve full swarm-like conditions is less than 100 μs. As a starting point we have calculated the EEPF that would give the same mean energy as measured for the "ON" period and we hope that it may represent the initial distribution reasonably well. The corresponding E/N giving the "right" mean energy (2.9 eV) is 60 Td. The E/N is evidently below the estimated effective E/N (but field in the ON period) which is mainly in the sheaths and in the bulk the field is small or negligible.

If we allow the initial EEPF to relax in zero field as one would expect in the afterglow the decay of the EEPF would occur over several μs as can be seen in fig. 4. Such fast decay of the EEPF is inconsistent with experimental observations so we have performed calculations with E/N as a function of time as given by the experimental data in fig. 2(b).

We show the calculated EEPF relaxation in BF_3 in fig. 5. The cross-sections of BF_3 were used in our model. The results display the same persistence of the mid-range EEPF (around 2 eV) over the time and similar mean energies. The EEPF thermalizes beyond 250 ms only when the effective E/N becomes considerably lower. In fig. 6 we show the time dependence of collisional processes in the afterglow. Initially rates of some processes, especially those requiring high excitation energy, are reduced but they recover as E/N becomes significant. As the field drops to low values, all rates also become smaller after 240 μs.

Kinetics of negative ions. – During the first stage of the afterglow, electrons dominate plasma diffusion and

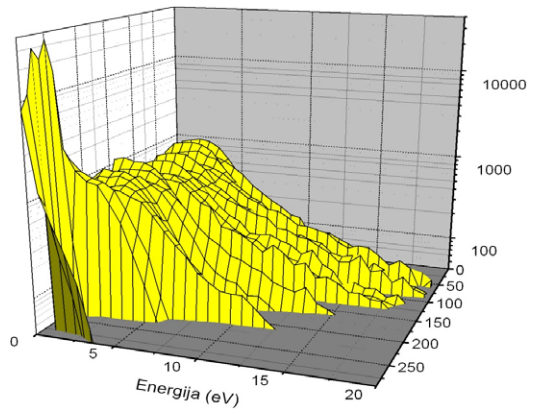

Fig. 5: (Colour on-line) Calculated EEPF relaxation in BF_3.

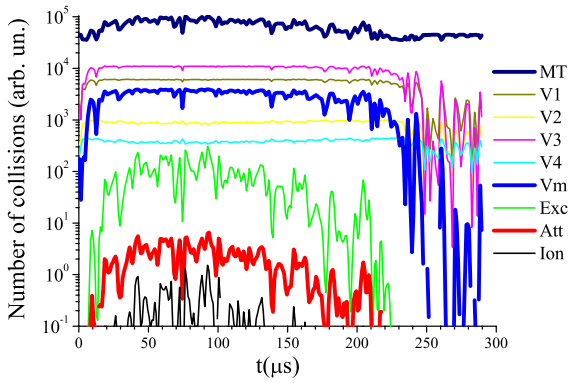

Fig. 6: (Colour on-line) Number of collisions in BF_3.

negative ions are trapped by the space charge potential inside the plasma. The flux of negative ions to the walls is nearly zero. During the second stage of the afterglow, electron density quickly diminishes, and positive and negative ions diffuse to the walls.

When detachment is important in the afterglow weakly electronegative gases like (BF_3), the plasma decay crucially depends on the product of negative-ion detachment frequency (γ_d) and diffusion time (τ_d). In the case $T_i \ll T_e$, the spatiotemporal dynamics is more complicated due to the presence of negative-ion density fronts during the afterglow, although negative ions diffuse freely in the plasma core, the negative-ion fronts propagate towards the walls with a nearly constant velocity. The evolution of ion fronts in the afterglow of electronegative plasmas is important, since it determines the time needed for negative ions to reach the wall, and thus influence surface reactions in plasma processing.

For a number of reasons one may wish to employ negative ions and hence pulsed operation with extended afterglows allowing extraction of negative ions.

The negative ions in pristine BF_3 are created by high-energy electron attachment, so they can be formed only during the pulse-ON. Therefore in the afterglow the low-energy electrons are expected to be lost by diffusion and not by attachment to BF_3. The electron loss process is slow and the negative ions are trapped by the remaining space charge field. From our results for the electron density in fig. 5 one may conclude that up to about 150 μs electrons dominate as negative charge carriers [3].

BF_3 plasma electronegativity is based on F^- and BF_4^- ions production. Although F^-, F_2^- and BF_2^- ions can be produced by the electron impact for energies above about 10 eV, only F^- ions are produced with significant abundance by the electron dissociative attachment [9]. In collisions of F^- and F_2^- ions with BF_3, BF_4^- ions are produced. The association reaction [10] is regarded to be the most important in the afterglow:

$$F^- + BF_3 \rightarrow BF_4^- .$$

The number density of F^- and BF_4^- ions is hard to predict in the pulsed BF_3 discharge afterglow due to the poorly known reaction rates. Since F^- ions undergo detachment with BF_3 at minimum energy of 4.35 eV these ions and clusters formed around the F^- ion [11] could be responsible for electron production in the afterglow. Influx of the electrons close to the energy of about 4.35 eV is visible in EEPF in fig. 2 only in the afterglow measurement.

Super halogen BF_4^- ions are very stable with respect to detachment [12] and one may expect that these heavy ions are present in the afterglow in the long term diffusing toward walls.

It is also worth mentioning that due to the shift of mean electron energy from very high values to lower energies one may expect that in the afterglow (especially with the persistent electric fields) attachment to radicals that have a low-energy threshold for dissociative attachment or thermal attachment may actually cause an increase of attachment.

It has been observed by experiment that the flux of negative ions grows in the afterglow. The observation is consistent with the discussed collapse of the field in the discharge and transition to free diffusion of ions.

However, another possible explanation for the observed peak in the measured negative ions in the afterglow could be related by attachment to some of the radicals or products of plasma chemistry that may have low or thermal attachment. This process would [13] create a large low-energy attachment to radicals since the BF_3 itself has a very high threshold for dissociative attachment. Since we do not have cross-sections for possible radicals and molecular products we will use a model mixture of BF_3 and F_2 to show how this effect develops.

In fig. 7 we show the temporal change in the rate of attachment in the ON period (modeled by effective E/N yielding the same mean energy as the discharge) and in the OFF period. F_2 is taken as a prototype of a radical with low-energy attachment and one can see that attachment actually increases in the OFF period. It is thus interesting to carry out an analysis of cross-sections for BF_x radicals

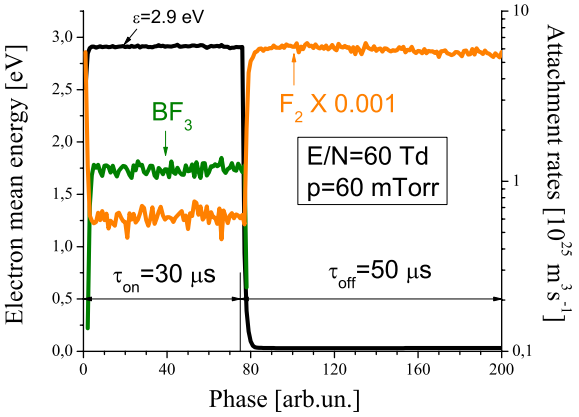

Fig. 7: (Colour on-line) Calculated electron mean energy in mixtures BF_3 and F_2.

similar to that done for CF radicals [13] and a similar analysis for the reaction rates [14].

Conclusion. – Time dependence of the mean electron energy and EEPF for a given reduced electric field (E/N) is being measured and calculated for the conditions of PLAD. We also discuss relaxation times and shape of the EEPF with and without electric field. A comparison between the calculated EEPF and the experimentally determined one reveals details of the electron dynamics in the pulsed DC regime.

The pulsed DC discharge in pure BF_3 consists of two stages pulse-ON and pulse-OFF. During the first stage high-voltage pulse across the anode and cathode gap drives the ionization and generates the population of electrons in the bulk which has a relatively small field. The high-energy electron population is responsible for the high ionization efficiency seen in the experimentally determined EEPF. A very high electric field across the cathode sheath induces the non-local character of the EEPF.

At the energies below 1.5 eV EEPF does not show the characteristics of a Maxwellian distribution although a slope up to about 2 eV (region I in figs. 3 and 4) may be fitted by a Maxwellian. Electron swarm simulations start with the experimentally determined mean electron energy $\langle e \rangle$ and calculates time relaxation of the EEPF for effective E/N during the pulse-ON period and for the measured time-dependent residual E/N in the pulse-OFF period. The EEPF relaxation obtained in the simulation and experiment agree well indicating that the relatively high mean energy of electrons in the afterglow is due to the residual electric field provided by an imperfect power supply. This residual field will have consequences for the rates of inelastic processes in the afterglow ionized gas. The number of collisions determined from the simulation is consistent with the momentum transfer and the vibrational excitation playing the main role in the momentum and energy balances and ionization by very-high-energy electrons in charged particle production, while drift, diffusion and to some degree attachment are the main loss mechanisms.

This paper provides an example of how the swarm technique may be used to model some aspects of realistic plasma devices and how the complex knowledge of time-dependent rate coefficients is important in such models [15,16].

* * *

The work presented here was supported in part by MNTRS 171037 project.

REFERENCES

[1] Radovanov S. and Godet L., *Workshop on Nonequilibrium Processes in Plasma Physics and Studies of the Environment*, *J. Phys.: Conf. Ser.*, **71** (2007) 012014, doi:10.1088/1742-6596/71/1/012014.
[2] Koo B.-W., Fang Z., Godet L., Radovanov S. B., Cardinaud C., Cartry G., Grouillet A. and Lenoble D., *IEEE Trans. Plasma Sci.*, **32** (2004) 456.
[3] Kaganovich I. D., Ramamurthi B. N. and Economou D. J., *Phys. Rev. E*, **64** (2001) 036402.
[4] Radovanov S., Godet L., Dorai R., Fang Z., Koo B. W., Cardinaud C., Cartry G., Lenoble D. and Grouillet A., *J. Appl. Phys.*, **98** (2005) 113307.
[5] Hopkins M. B. and Graham W. G., *Rev. Sci. Instrum.*, **57** (1986) 2210.
[6] Singh H. and Graves D. B., *J. Appl. Phys.*, **87** (2000) 4098.
[7] Šašić O., Petrović Z. Lj., Raspopović Z., Godet L. and Radovanov S., *58th Annual Gaseous Electronics Conference, October 16–20, 2005, San Jose, California*, *Bull. Am. Phys. Soc.*, **50** (2005) 65, UH2 4.
[8] Petrović Z. Lj., Marković V. Lj., Pejović M. M. and Gocić S. R., *J. Phys. D: Appl. Phys.*, **34** (2001) 1756.
[9] Stockdale J. A., Nelson D. R., Davis F. J. and Compton R. N., *J. Chem. Phys.*, **56** (1972) 3336.
[10] Herd C. R. and Babcock L. M., *J. Phys. Chem.*, **91** (1987) 2372.
[11] Zhao X.-L. and Litherland A. E., *Nucl. Instrum. Methods Phys. Res. B*, **259** (2007) 224.
[12] Gutsev G. L., Jena P. and Bartlett R. J., *Chem. Phys. Lett.*, **292** (1998) 289.
[13] Rozum I., Limao-Vieira P., Eden S., Tennyson J. and Mason N. J., *J. Phys. Chem. Ref. Data*, **35** (2006) 267.
[14] Nikitović Ž., Stojanović V., Petrović Z. Lj., Cvelbar U. and Mozetič M., *EPL*, **91** (2010) 55001.
[15] Petrović Z. Lj., Šuvakov M., Nikitović Ž., Dujko S., Šašić O., Jovanović J., Malović G. and Stojanović V., *Plasma Sources Sci. Technol.*, **16** (2007) S1.
[16] Petrović Z. Lj., Dujko S., Marić D., Malović G., Nikitović Ž., Šašić O., Jovanović J., Stojanović V. and Radmilović-Rađenović M., *J. Phys. D: Appl. Phys.*, **42** (2009) 194002.